5-2016

Devitrification Rates of Fused Silica in the Presence of Trace Impurities

Nicholas Kivi
University of Tennessee, Knoxville, nkivi@vols.utk.edu

Adrian Moore
University of Tennessee, Knoxville

Kayla Dyar
University of Tennessee, Knoxville

Samuel Haaf
University of Tennessee, Knoxville

Devitrification Rates of Fused Silica in the Presence of Trace Impurities

Team: Sam Haaf, Kayla Dyar, Adrian Moore, Nick Kivi
Mentors: Maulik Patel, Kurt Sickafus
Department of Materials Science and Engineering
University of Tennessee, Knoxville
Industry Collaborator: Rod Haaland
Alcoa Power and Propulsion
Senior Design MSE 489
April 27, 2016

1. Abstract

Ceramic cores can be used in the investment casting process to produce a product that will be hollow or contain holes. Alcoa Howmet produces the cores that are used to make the hollow air channels that provide internal cooling to the blades that are used in jet engines and power generation turbine blades. The material of choice for the cores is SiO_2 due to its low thermal expansion coefficient, and a high melting temperature. This project sought to demonstrate the effects of trace amounts of three different dopants (Ti, Al, & K) on the devitrification of fused silica into the cristobalite phase of SiO_2. It also examined the effect of different processing techniques (ball milling and v-cone milling with alumina and silicon nitride milling media respectively) on the devitrification of fused silica and the formation of cristobalite phases in SiO_2. *In-situ* high temperature X-ray diffraction (HTXRD) was used to analyze the phase transformations and the cristobalite growth rate as a function of temperature. HTXRD shows that doping fused silica to analyze the phase transformations as a function of temperature indicates which dopant has the greatest effect on the material. Inductively coupled plasma mass spectrometry (ICPMS) shows the precise elemental composition of the samples being analyzed and the contamination from the milling media. Analysis of data showed that potassia has a significant effect on the devitrification of fused silica, while alumina and titania did not. There was not any evidence to suggest that the media of the ball milling made any significant difference in devitrification. Finally, the experiment highlighted the need for an accurate method for determining of crystalline versus amorphous content for successful industrial replication in the future.

2. Introduction

2.1 Ceramic Cores

Many industries, such as chemical, manufacturing and power, desire high performance ceramics that can withstand corrosion and extreme temperatures such as Alcoa. Engineering materials that possess these properties can often be the factor that lands a contract to fabricate high performance devices for the military or other industries that demand high quality performance . This desire to engineer the best ceramics can specifically be seen in the industry of investment casting superalloys for turbine blades.

Alcoa-Howmet is responsible for producing ceramic cores. A typical ceramic core can be seen in Fig. 1. Ceramic cores have an intricate design full of holes and channels that allow internal cooling for jet and power-generation turbine blades. These cores must have a high melting temperature to withstand the heat during the casting process, and low thermal expansion for having high tolerances in the design aspect of ceramic cores. To achieve this the cores utilize different phases of SiO_2, such as cristobalite and fused silica. Fig. 2 shows the temperature versus pressure phase diagram of silica under equilibrium conditions. The cristobalite phase forms at atmospheric

pressure and at temperatures over 1450°C. However, when fused silica devitrifies due to the presence of impurities, the first phase that forms below the melting temperature, is cristobalite. Devitrification is the process of crystallization in a crystal-free amorphous glass which includes holding at high temperature for a long time, which causes the nucleation of crystals [1].

Figure 1 - *Ceramic pattern for jet turbine ceramic cores. The piece is placed in a turbine pattern before it is filled with wax. An investment is made and the wax is burned out, leaving the ceramic core in the hollow shell. Once the product is cast, the core is dissolved with acid and the final turbine has a hollow center to allow internal air flow [2].*

2.2 Phases of Silica

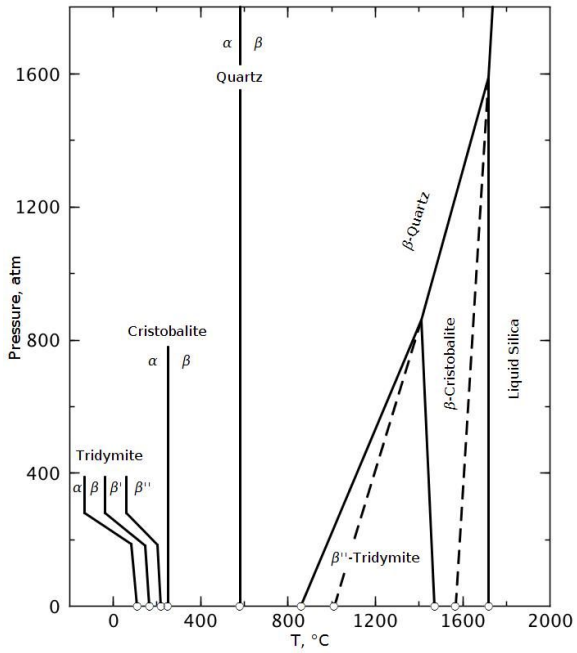

Figure 2- *The phase diagram for SiO_2 as a function of temperature and pressure. The cristobalite phase precipitates at 1450°C and at atmospheric pressure [3].*

The different phases of silica are used to control the volumetric expansion during the casting process. Fused silica is a non-crystalline glass form of silica made from high purity sand deposits. It has a very low thermal expansion ($0.55 * 10^{-6}$ /°C), high thermal shock resistance. Phase transformations of fused silica at different temperatures can be found in Table 1. Below 867℃, fused silica is stable. Fused silica devitrifies above 1100℃ into cristobalite through a transitional amorphous phase. Above 1450℃, cristobalite is the stable phase. Cristobalite is found in powder form at room temperature due to its metastable properties. Transitioning to cristobalite in the 867-1450℃ range creates a metastable cristobalite phase that can be used for processing purposes [4].

Table 1*- Phase Transformations in Fused Silica [4]*

Temperature Range(s)	Transformation
Below 867℃	No transformation, stable.
867℃ - 1450℃	Devitrifies above 1100℃ into cristobalite
Above 1450℃	Stable cristobalite

The mineral cristobalite is a high-temperature polymorph of silica. In turbine blades such as Figure 4, a silica core that has a composition of primarily alpha-cristobalite can experience a phase transformation into beta-cristobalite when it comes into contact with the heat of the molten metal cast. The phase change creates a volumetric expansion which, when the mold cools, will fracture the product as shown in Fig. 3. This is addressed in manufacturing by creating cores that have a specific concentration of alpha-cristobalite, a proprietary composition used by Alcoa-Howmet, and the remainder is fused silica. The compound silica, SiO_2, has 22 modes of which 17 are crystalline and 5 are amorphous. Fused silica glass has a very low thermal expansion coefficient and is thermally shock resistant.

Figure 3- *A wax pattern of a jet engine turbine blade. The ceramic core is already fixed in this pattern, and the final product will bear these same dimensions [5].*

In cristobalite, SiO_2 tetrahedra are joined corner to corner in order to form long range order, as seen in Figure 4a and 4b. The crystallization, or devitrification, of fused silica to cristobalite begins at the surface and works inward. Higher temperatures give the amorphous silicates enough energy to create bonds and form structures. Impurities added to fused silica can accelerate the devitrification rate of silica into cristobalite [4].

Cristobalite itself has two polymorphs: alpha and beta cristobalite. Alpha cristobalite is a low temperature polymorph that transforms into beta cristobalite via a reversible inversion at approximately 270℃ [4]. Both alpha and beta cristobalite have very similar octahedral structures, however alpha cristobalite has a tetragonal symmetry and beta cristobalite has an isometric symmetry. Due to the similar structures, there is a small volumetric change during the transition. This is addressed in manufacturing by creating cores that have a specific concentration of alpha-cristobalite, a proprietary composition used by Alcoa-Howmet, and the remainder is fused silica. A typical mix will have anywhere from 15-20% alpha cristobalite. This must be accounted

for in the casting process to increase precision of the design. If the ratio is incorrect, there can be structural weakening or complete fracture in the product when the cast cools.

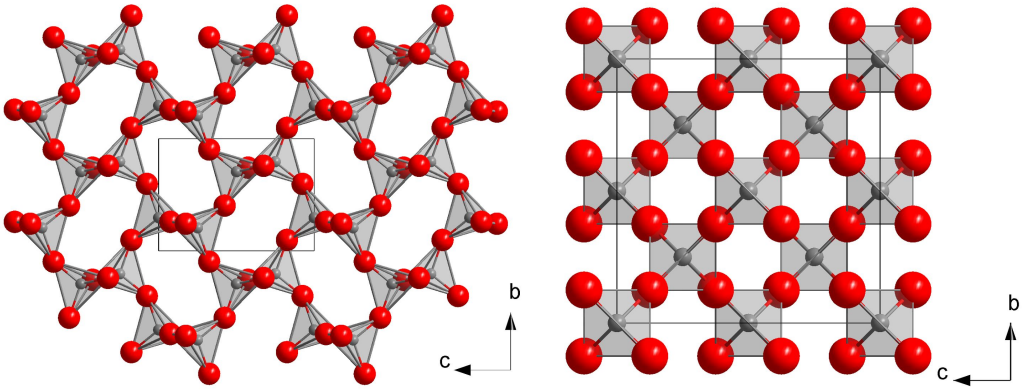

(a) (b)

Figure 4: *(a) Alpha cristobalite crystal structure: octahedral with tetragonal symmetry (b) Beta cristobalite crystal structure: octahedral with isometric symmetry [6]*

In the simple structure of SiO_2, as shown in Figure 5 and 6, silicon is the basis of the tetrahedra on which the network is formed, which is known as the network former. Two oxygen atoms are present within the network which link other tetrahedra together, which are known as bridging atoms. Oxygen atoms that do not link other tetrahedra together are considered non-bridging atoms. The elementary structure of silica can be seen in Figure 5. When an impurity of different composition is introduced into the network, atoms of the impurity can act as network modifiers that can support and change the shape of the silicate network, as seen in Figure 6. The addition of impurities will essentially alter the network, potentially changing a material's mechanical and thermal properties. This is the cause for great importance in choosing the correct dopants.

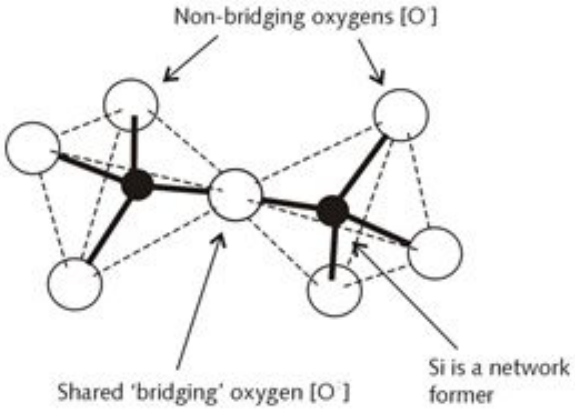

Figure 5- *Simple structure of* SiO_2.

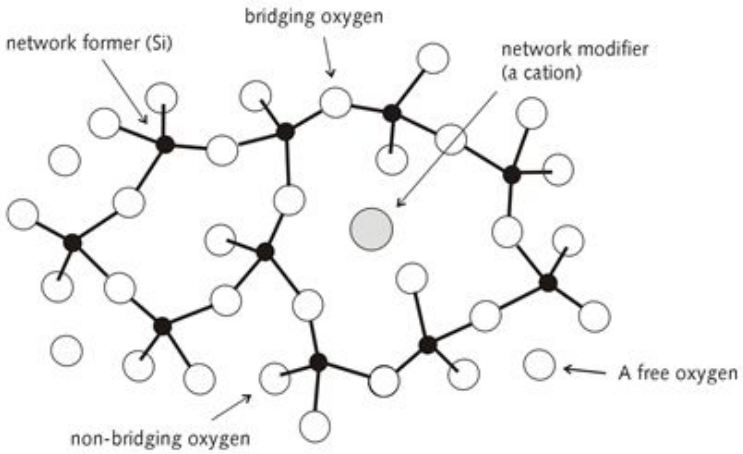

Figure 6- *The structure of* SiO_2 *showing silicon being the basis of the tetrahedra on which the network is formed.*

2.3 Investment Casting

Investment casting, also known as lost wax or lost foam casting, dates back thousands of years to around 1100 A.D. [5] The process is an ancient technique that has been refined and engineered into a modern day highly technical process which is illustrated in Figure 3. The process begins with a master pattern that is formed into the shape of the final product. From that pattern, the master die, which can be used in the processing of hundreds of products, is formed out of a low-melting point metal or steel. At this point, any ceramic core that will be in the final product can be inserted into the die and the die is filled with wax. The pattern is removed from the die and an investment cast is made. First the pattern is dipped into a slurry of a finely grained ceramic. Once the excess slurry drips off of the mold, it is either dipped into a more coarsely grained ceramic slurry or a ceramic paste is applied by hand . The investment is left to harden for several hours, and the process is repeated until it has reached the desired thickness. Once complete, the investment is heated in the furnace for several hours to further harden the ceramic and to burn out the wax. The molten metal of the turbine blade is then poured into the hollow mold with the ceramic core in place.

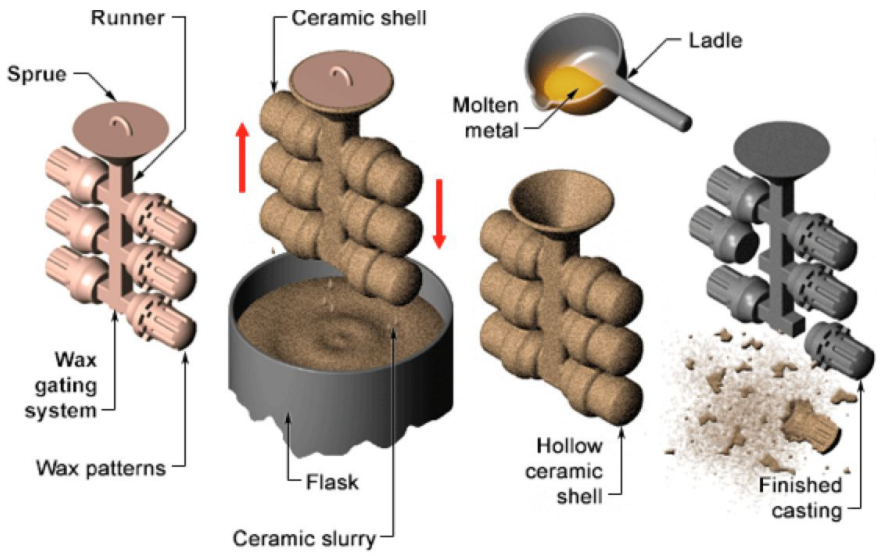

Figure 7- *The process of lost wax, otherwise known as investment casting. The wax is dipped into a ceramic slurry to create the investment, then the wax is burned out. Molten metal is poured into the investment mold, and once the metal has hardened the shell is broken away to reveal the product [7].*

Cristobalite is used in combination with fused silica in order to minimize thermal expansion of the core during the pouring process. Without cristobalite, the molten metal would cause too much expansion in the cast, which could lead to stress centers and premature failures in the part. By using preset amounts of cristobalite and fused silica, the kinetic energy from molten metal will convert some of the fused silica to cristobalite and reduce the thermal expansion. By using different dopants and different compositions, the rate of cristobalite growth can be increased or decreased accordingly.

During the processing of the silica cores, SiO_2 powder is ball milled with small quantities of impurities to affect the rate of formation of cristobalite. The ball mills are made of materials that contribute to the impurity concentrations in the powder sample, which must be taken into consideration. The harder the ball-mill material is, the less it contributes to the composition of the product. The techniques that are utilized include *in situ* HTXRD to analyze the phase transformations as a function of temperature. ICPMS is used to determine the precise elemental composition of the samples being analyzed and the contamination from the milling media. This project is important for the reasons of improving the process of investment casting. This project seeks to demonstrate the effects of trace amounts of three different dopants (Ti, Al & K) on the devitrification of fused silica into the cristobalite phase of SiO_2. It also examines the effect of different processing techniques on the devitrification of fused silica and the formation of cristobalite phases in SiO_2.

3. Experimental Procedure

3.1 Introduction

The experimental process began with preparing eighteen samples, whose compositions can be found in Table 2. The quantities of each material used to prepare the samples were determined using Eq. 1. FS indicates fused silica, C indicates cristobalite, and I indicates the impurity that was introduced. The dopants that were chosen can act as network modifiers in glass and contribute to the devitrification of the fused silica.

$$FS/C/I = ((\text{Atomic \% (FS)} * (\text{mol/20g}) * 60.08) * 10 \qquad \textbf{Equation 1}$$

Table 2- *Samples and their amounts that were used.*

Metal Oxide	Fused Silica (g)	Cristobalite (g)	Metal Oxide (g)
TiO_2 (0.12%)	**170.29**	**29.40**	**0.31**
TiO_2 (0.23%)	**170.03**	**29.36**	**0.62**
TiO_2 (0.35%)	**169.77**	**29.31**	**0.92**
Al_2O_3 (0.12%)	**170.22**	**29.39**	**0.39**
Al_2O_3 (0.23%)	**169.88**	**29.33**	**0.78**
Al_2O_3 (0.35%)	**169.55**	**29.28**	**1.18**
$KHCO_3$ (0.12%)	**170.22**	**29.39**	**0.39**
$KHCO_3$ (0.12%)	**169.90**	**29.33**	**0.77**
$KHCO_3$ (0.12%)	**169.57**	**29.28**	**1.15**

* Samples were prepared in 200 g batches

The sample preparation procedure was constant and did not change throughout making the samples. In order to explore the effects of two different sample preparation techniques, sample preparation was performed on nine samples in UT's laboratory and nine samples at Alcoa-Howmet. Fig. 8 represents the sample preparation at Alcoa while Fig. 9 represents the sample preparation at UT. The procedure began with measuring each powder out by the weights shown in the appendix with percent compositions of each sample being 0.12%, 0.23%, and 0.35%. Each quantity was weighed out using a laboratory scale and placed in a container where it was transferred to a ball mill for mixing. It is to be noted that the samples that were prepared at UT were calcined prior to ball milling. For each powder sample, a small portion was collected and shipped to a laboratory that

performed ICPMS for precision composition analysis. This was done to check the precision of the powder making process. The samples were calcining for two hours at 200°C. Once the samples were weighed at each location, they were poured into a silicon nitride ceramic vial and and alumina ceramic vial at UT and Alcoa, respectively. The silicon nitride vial operates with two silicon nitride milling balls, and the alumina vial rotates at low energy with numerous alumina milling pellets. Ball milling was performed with isopropanol for 90 minutes in UT's powder preparation lab and for 60 minutes at Alcoa- Howmet with deionized water. A ceramic jar was used for ball milling at Alcoa Howmet. Experimental powder, Al_2O_3 milling media, and deionized water were added to create the milling slurry. At UT, the container was an SPEX Sample Mixer and Mill to ball mill experimental powders. Si_3N_4 media and isopropanol were used to ball mill for an hour and a half.

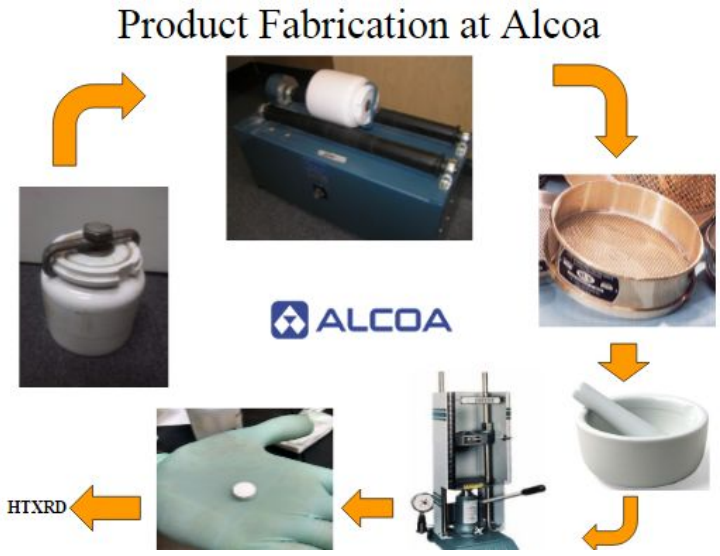

Figure 8: *A visual representation of Alcoa's product fabrication can be seen with different processing factors than UT.*

Figure 9: *A visual representation of UT's product fabrication can be seen with different processing factors than Alcoa.*

When the milling process was complete, the ceramic jars were removed from the ball mill and prepared for the drying stage. At Alcoa, the jar was emptied into a sieve to separate the slurry from the milling material. The liquid slurry was then transferred to the furnace where it was dried for 24 hours at 81°C. After drying, it was crushed in a mortar and pestle and stored for transportation back to UT. For the samples prepared at UT, the drying process only involved opening the vials and waiting 8 hours for the isopropanol to evaporate. The samples were then crushed in a mortar and pestle and stored for later analysis. Once again, small collections of each sample after milling were sent off for ICPMS analysis in order to see if the ball milling process changed the elemental composition of the powders.

After the powder dried, approximately 10 grams of powder were placed into a Carver Press and applied with approximately 5000 lbs of force in order to pelletize. The press and pellet chamber were washed pre-pelletization with isopropanol in order to remove all potential unwanted impurities.

3.2 High Temperature X-ray Diffraction (HTXRD)

In order to determine the different amounts of cristobalite formed at certain temperatures, HTXRD was performed. Fig. 10 shows the PANalytical Empyrean fitted with a high temperature stage. The Cu K_{α} incident beam is generated on the left in the X-ray tube. The beam passes through standard soller slits and enters the high temperature stage, in the center, through a window made from two foils: an inner foil of graphite that contains the heat of the furnace and allows X-rays to pass, and outer foil of Kapton, a yellow polymer that allows the passage of X-rays. The X-rays diffract off of the pellet sample and pass back through the window. The PIXcel detector collects the

radiation in 1D scanning mode at different angles while the detector and X-ray source rotate around the sample.

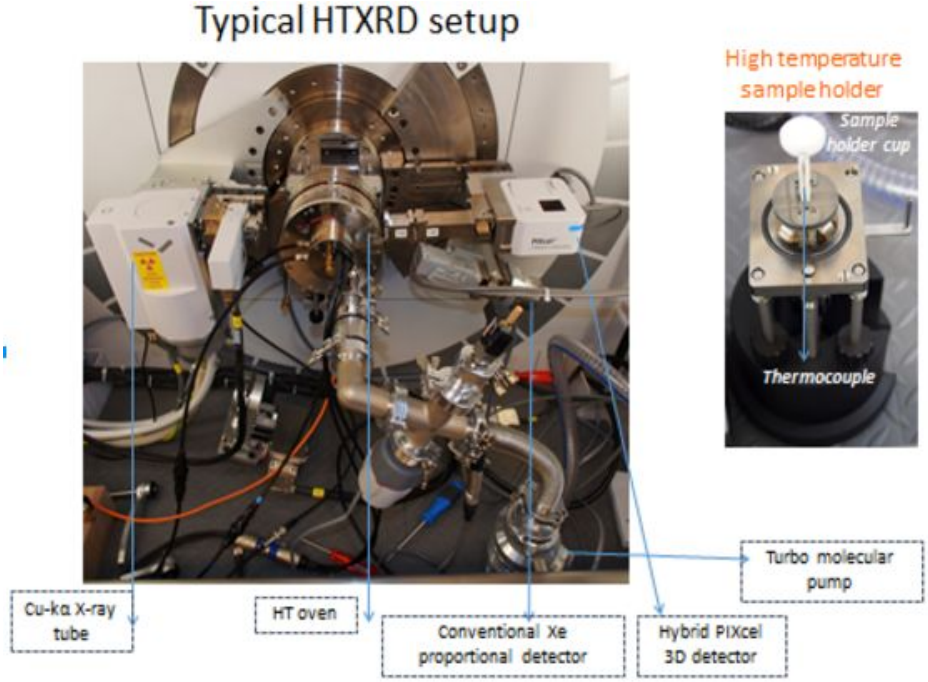

Figure 10- *The PANalytical Empyrean ran the HTXRD scans on the powder pellets. The incident beam is produced in the X-ray tube on the left side of the instrument, the high temperature sample stage is in the center of the instrument, and the diffracted beam is collected by the PIXcel detector on the right side of the instrument. [9].*

Fig. 11 shows the temperature profile for each sample. Before each XRD scan was run, the instrument must be calibrated and aligned to the individual pellet. Once calibrated, the attenuator was removed and a batch script that contains the heating and scanning instructions was initiated. The whole HTXRD run makes a total of 11 XRD scans and takes a total of 10.5 hours. During scan, water was run through the heating chamber as a means of cooling the instrument internally to prevent the melting of the instrument. The temperature profile and the location of each of the scans can be seen in Fig. 11.

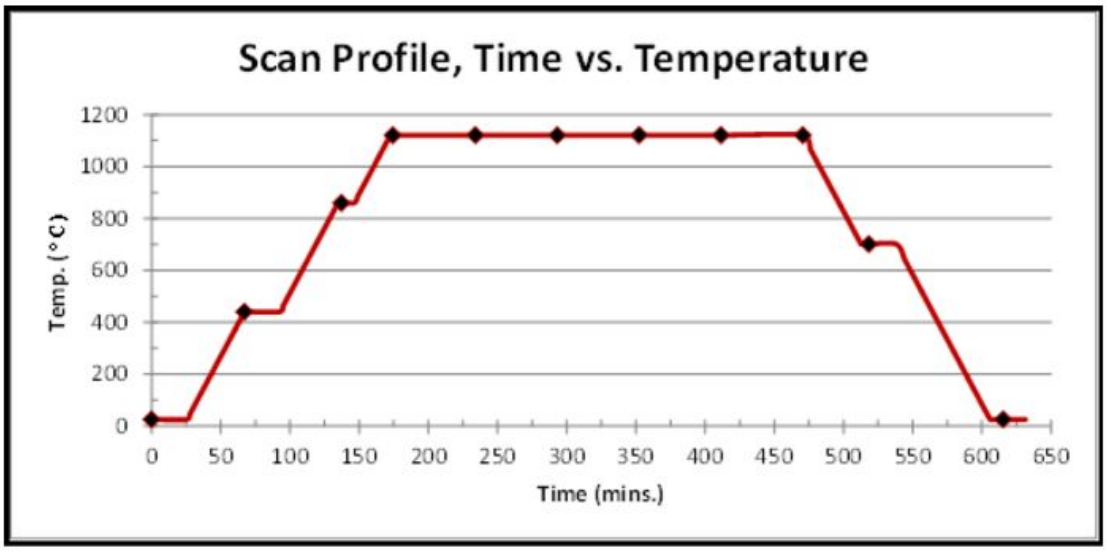

Figure 11 *- Temperature profile for HTXRD scans as a function of time. Each marker on the graph represents a point in the program where an XRD scan was recorded. [10]*

3.3 Data Analysis

The data collected was then analyzed using the statistical programming language R to determine the cristobalite concentrations at each step in the heating cycle. Two different methods were implemented in R to determine the amount of cristobalite present in the sample at each point during the heating profile.

The first method matches the amorphous background radiation with a quadratic fit model, and then subtracts the value for the amorphous background from the whole pattern. The remaining intensity profile was treated as that of the radiation detected from the cristobalite phase in the sample, and the intensity of the maximum peak was recorded. The ratio of the intensity of the maximum peak at each step in the HTXRD program to the intensity of the maximum peak in the initial room temperature scan was then multiplied by the initial concentration of cristobalite that was present in the sample, 15%, to get the instantaneous composition, as seen in Eqn. 2.

$$\%\ Cristobalite\ =\ I/I_0\ X\ 15\% \qquad \textbf{Equation 2}$$

The second method was implemented in order to find a more scientifically grounded method of determining the precise concentration of cristobalite at each phase. The motivation was found in observation of the hump in the fused silica XRD profile that centers around the highest intensity peak location of cristobalite. There was a normal distribution of d-spacings in the amorphous content with a mean of the d-spacing centered around that of the cristobalite peak was theorized, and that as the amorphous phase devitrifies, the hump will resolve and the intensity of the

cristobalite peak will increase. The integration of this whole region should then stay constant throughout the whole transformation.

The first step was to use a function to match the background radiation, and then to subtract the background from the whole profile. Then the peak and the surrounding area was integrated to get the intensity of the whole region, and which the peak was integrated by itself to get that intensity. The ratio of the integration of the peak to the integration of the whole region was considered to be the concentration of cristobalite. This process is illustrated in Fig. 12.

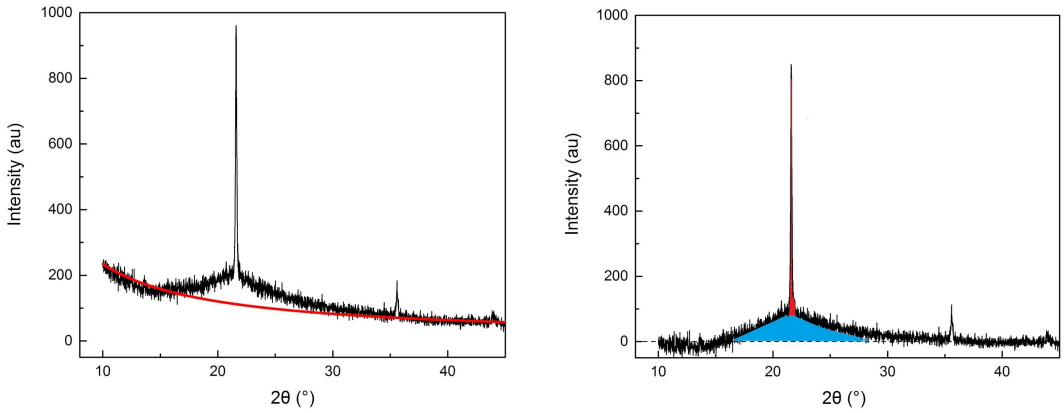

Figure 12 - *The 0.23 mol% K_2O sample at 440°C. (left) The background was fit as a function of $(2\theta)^{-1}$. (right) The background was subtracted. The blue and red regions are integrated together to get the intensity contributed by both the fused silica and the cristobalite. The red region was integrated by itself to get the intensity contributed by the cristobalite alone. The ratio of the red region to the combination of the red and blue regions are used to determine the concentration of cristobalite.*

4. Results & Discussion

Fig. 13 shows the XRD profile of each of the materials used in this experiment taken at room temperature. When the samples are prepared in the concentrations listed in Table 2, their XRD profile at room temperature looks like the one shown in Fig. 14. When compared to the profiles of the individual constituents shown in Fig. 13, it can be seen that the profile contains the amorphous profile of the fused silica and the crystalline peaks of the cristobalite, but none of the peak from any of the dopants. This was to be expected, as the dopants are present in such small concentrations that their effect can not be seen on the XRD profile directly; there must be at least 3% of a material present to see its diffraction pattern. In Figure 13, note how the fused silica has an

increase from background distribution centered around the (101) peak of cristobalite. As fused silica devitrifies into cristobalite, this region resolves into the crystalline peak of the cristobalite.

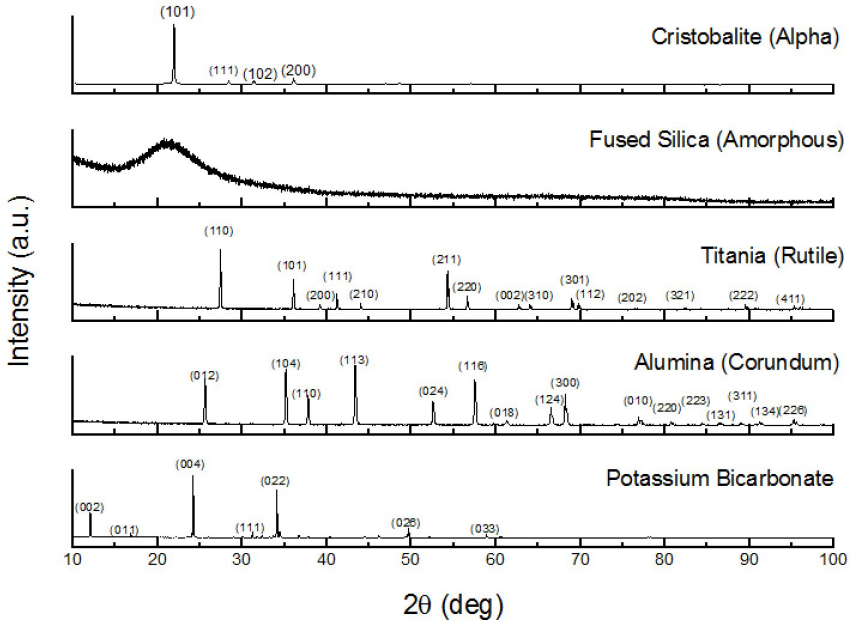

Figure 13 - *Reactant Powder XRD results for alpha cristobalite and amorphous fused silica with reference rutile structured titania [13] , corundum structured alumina [14] and potassium bicarbonate [15]. Reference patterns were found using the Inorganic Crystal Structure Database (ICSD).*

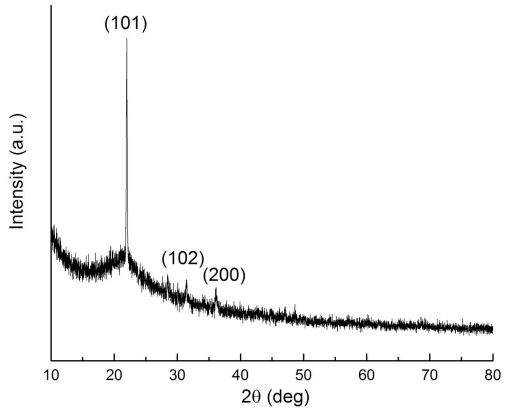

Figure 14 - *An example XRD spectra at 25 ℃ from 10° to 80° 2θ in the .12 mol% TiO_2 sample prepared at UT's sample preparation lab. This profile was observed in all of the XRD scans taken with differences in the primary peak intensity and the background radiation.*

Fig. 14 shows the complete XRD spectra taken at 25°C on the .12 mol% TiO_2 sample in the 2θ range of 10-80°. The amorphous structure of the fused silica is responsible for the background intensity in the lower 2θ range. The (101) peak of cristobalite as well as two secondary peaks , (102) and (200) were visible due to the initial cristobalite content.

When the XRD profiles are observed as a function of temperature, the first noticeable effect was a transition of the primary peak from approximately 22.0°2θ to approximately 21.5°2θ, as seen in Fig. 15. When compared to ICSD standard diffraction patterns, these peaks match the (101) alpha-cristobalite and (111) beta-cristobalite peaks, respectively. This effect was explored more thoroughly by running another HTXRD profile at smaller temperature increments on a sample of pure cristobalite. Fig. 16 shows the profiles in the temperature range of 200°C to 250°C, and it can be seen that a transition of the sample from alpha-cristobalite to beta-cristobalite has started at 225°C. This corresponds with literature, which says that this transition occurs in the temperature range of 220°C to 290°C, as discussed in the introduction [4].

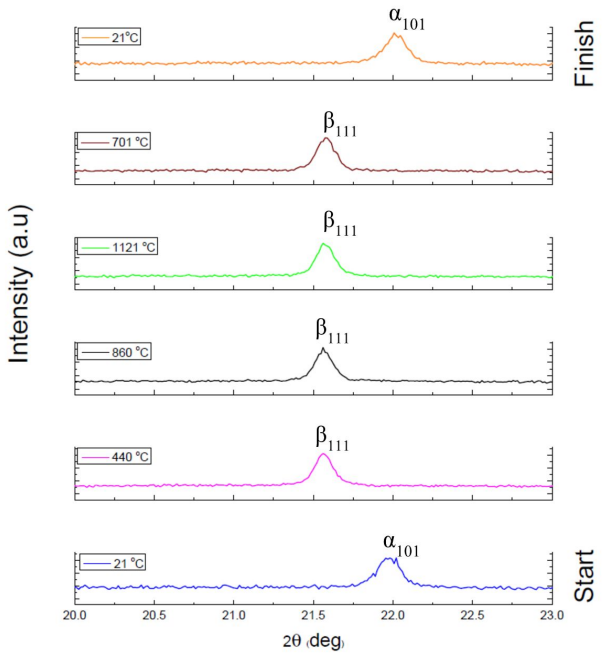

Figure 15 - *HTXRD volume expansion patterns for the UT 0.35 mol% K_2O samples throughout the heating profile. The shift from approximately 22.0° 2θ to 21.5° 2θ indicates a transition between alpha cristobalite and beta cristobalite [12].*

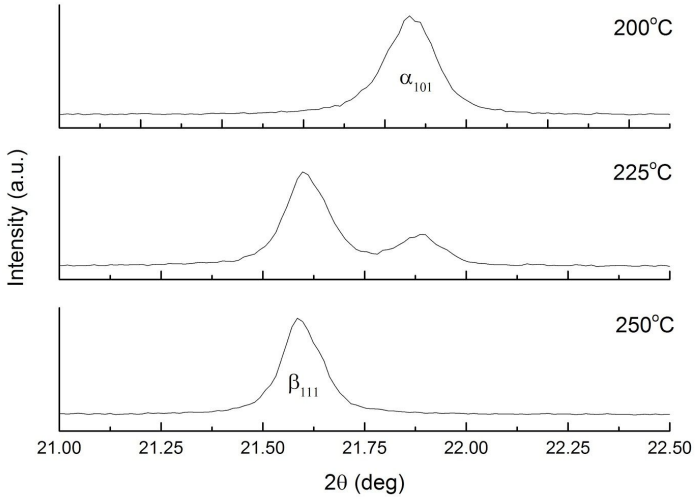

Figure 16 - *The profiles in the temperature range of 200°C to 250°C are shown above, and it can be seen that a transition of the sample from alpha-cristobalite to beta-cristobalite has started at 225°C.*

The second effect observed is that there was a minimal change in the intensity of primary cristobalite peak for all of the titania- and alumina-doped samples, as demonstrated with the 0.35 mol% TiO_2 sample in Fig. 17. The samples doped with potassia, however, demonstrate a significant transformation during the heating cycle, as seen in Fig. 18. This initial observation suggests that the introduction of potassia stimulates the devitrification of fused silica into the crystalline phase, cristobalite, and that the other two dopants do not. Potassia creates such a large intensity change that there is a very slight peak shift of approximately .2° 2θ. This was an unexpected result, as this peak shift would indicate volumetric reduction. Further experimentation will need to be done in order to identify what is occurring here. This aside, we are seeing intensity grow as a function of temperature, indicating devitrification of fused silica into cristobalite.

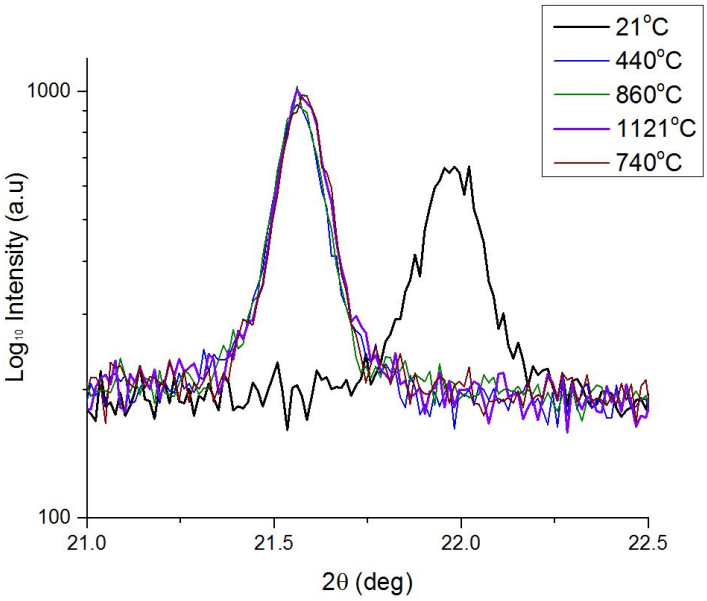

Figure 17 - *Overlaid spectra highlighting peak shift in the 0.35% TiO_2 sample from UT. The approximately 22° 2θ peak is the room temperature scan showing the (101) peak of alpha cristobalite, whereas the high temperature scans show the approximately 21.5° 2θ peak indicative of the (111) peak of beta cristobalite.*

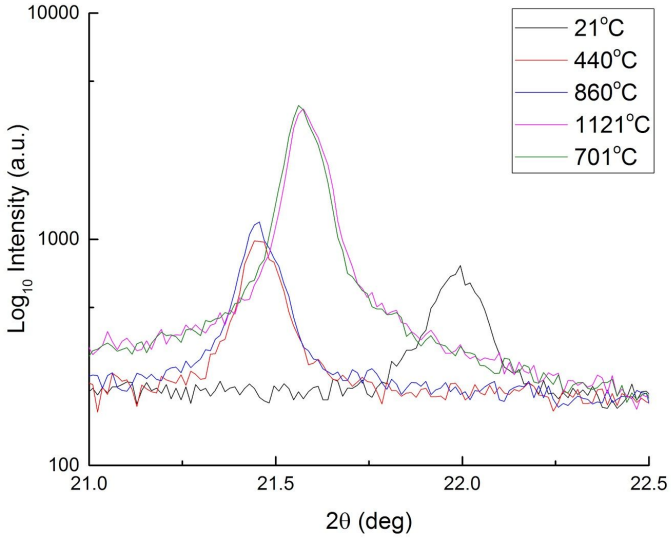

Figure 18- *Overlaid spectra highlighting peak shift in the 0.35% K_2O sample from UT. Higher temperatures show drastic intensity increases as well as a slight peak shift between 21°C and 440°C as well as 860°C and 1121°C The approximately 22° 2θ peak is the room temperature scan showing the (101) peak of alpha cristobalite, whereas the high temperature scans show the approximately 21.5° 2θ peak indicative of the (111) peak of beta cristobalite.*

A statistical analysis program, developed and run by Samuel Haaf, was used to analyze the intensity of the spectral peaks as a way of determining cristobalite growth and content. The code can be seen in the Appendix. Initially, the program matched a quadratic function to the amorphous

background curve, then subtracted the background from the profile. The intensity of the largest peak was recorded. Cristobalite content was determined by taking the ratio of the intensity of that largest peak to the initial largest peak from the room temperature scan and multiplied by the initial concentration of cristobalite from the experimental procedure, 15%. The data collected in this analysis run is shown in Fig. 19.

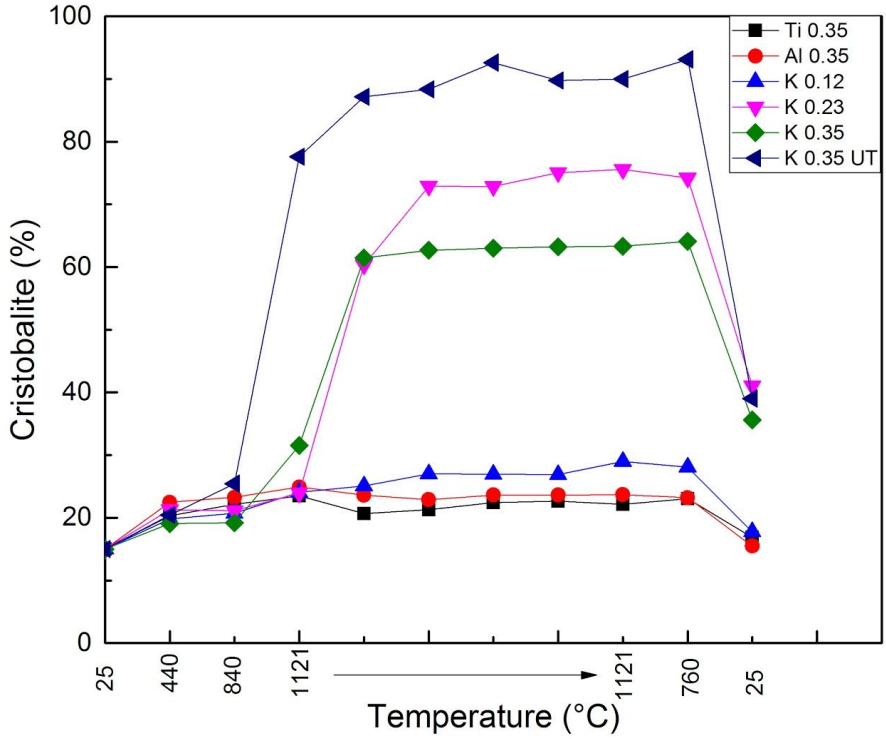

Figure 19 - *The results of the first data analysis method. Potassia has a large effect on the increase of cristobalite growth in fused silica, whereas alumina and titania have a nominal effect.*

The results of the first method seen in Fig. 19 show that the samples that were doped with the highest concentrations of titania and alumina demonstrated very little change in cristobalite concentration from the initial value of 15%. The potassia sample with the smallest dopant addition, 0.12 mol%, demonstrated a slightly higher cristobalite formation that the two samples mentioned previously. The most significant results are observed in the higher concentrations of potassia, 0.23 mol% and 0.35 mol%, which show more than double the cristobalite present than the three aforementioned samples. One surprising observation was that the 0.35 mol% sample prepared at Alcoa had a lower devitrification rate than the 0.23 mol% sample. The 0.35 mol% sample prepared at UT was plotted to see if it had a higher devitrification than the 0.23 mol% from Alcoa, and it did as expected.

A second analysis was done with a slight modification to the analytical process. Since, in theory, amorphous silica will devitrify into the cristobalite (101) peak, the amorphous background peak will resolve itself into the peak. This was quantified with the program by Haaf. The background of the scan outside of the region 5° 2θ to each side of the peak was matched with a

function of (angle 2θ)$^{-1}$. This fit, attributed to background radiation of the amorphous sample, was used to subtract the background from the whole profile. The area of the peak and the surrounding area, which was attributed to the normal distribution of d-spacings in the fused silica, was integrated. The area under the peak alone was integrated, and a ratio of this integration to the one of the whole region was taken to be the concentration of cristobalite in the sample. Those ratios are plotted in Fig. 20. as a percentage.

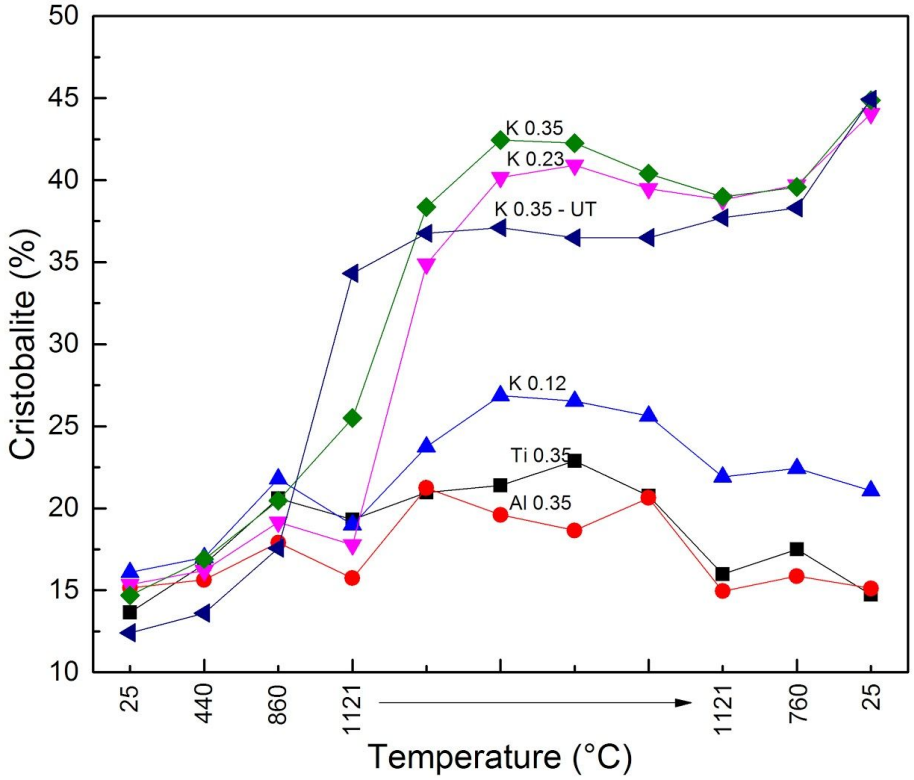

Figure 20 - *The results of the second data analysis method. Still, potassia has a large effect on the increase of cristobalite growth in fused silica, whereas alumina and titania have a nominal effect.*

The results of the second analysis method differ in some regards to the results of the first method. One of the primary differences was that the 0.35 mol% sample from Alcoa was determined to have had devitrified slightly more than the 0.23 mol% sample, as was expected from the beginning. The 0.35 mol% sample from UT was slightly lower than both of them, but since all three are very close in value, this may be due to experimental error. Another significant difference in the results is that the cristobalite concentration was in the range of 35 to 45% for the highly doped K_2O samples, whereas the first method showed concentrations of up to 95% forming. Both of the analysis methods, however, confirm that the devitrification of fused silica doesn't begin until the sample has exceeded a temperature of 1100°C.

The process that was used in the second analysis method is likely more accurate than first method because its process is based on a theory that the amorphous content, when it devitrifies into

cristobalite, will resolve into the crystalline peak. The first method also assumed that there was an initial composition of 15% cristobalite present in the sample, and the rest of the values were based off of that assumption. The second process did not assume that there was initially any cristobalite present in the sample, but still produced initial values of approximately 15%.

Devitrification was expected of glass modifiers, but not expected of glass networkers. Potassia is classified as a modifier, so it was expected to have caused devitrification. Alumina and titania are both considered glass intermediates, so they could have either behaved as modifiers or networkers. This study concludes that, for amorphous silica, both of these dopants behave as networkers, not modifiers.

The effect of milling media on the compositions of the samples can be observed in Figs. 21 - 24. Fig. 21 and Fig. 22 are the results of the ICPMS compositional analysis on the TiO_2 doped samples prepared at UT and Alcoa, respectively. Both of these figure show an unexpected presence of Al_2O_3. Its presence in both of the samples in roughly equal quantities suggest that the cristobalite, the fused silica or both of the starting materials contain Al_2O_3 as an impurity. This impurity did not contribute to the devitrification rate though because, as discussed earlier, Al_2O_3 is not acting as a network modifier. All four of these figures confirm that each of the samples were doped with the material that they were claimed to have been doped with. The TiO_2 doped samples, however, have unexpected compositional distributions. Two of the samples prepared at UT appear to have the same composition, and the 0.23 mol% sample prepared at Alcoa has a higher concentration of Ti than the 0.35 mol% sample. Ti was determined to not have an effect on the devitrification rates, so these compositional errors do not have significant impact on the study.

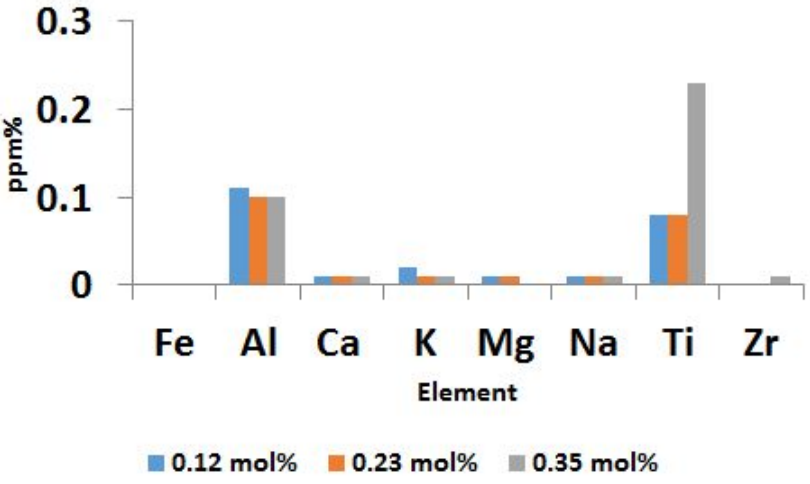

Figure 21 - *Results of ICPMS analysis on the titanium-doped samples prepared at UT.*

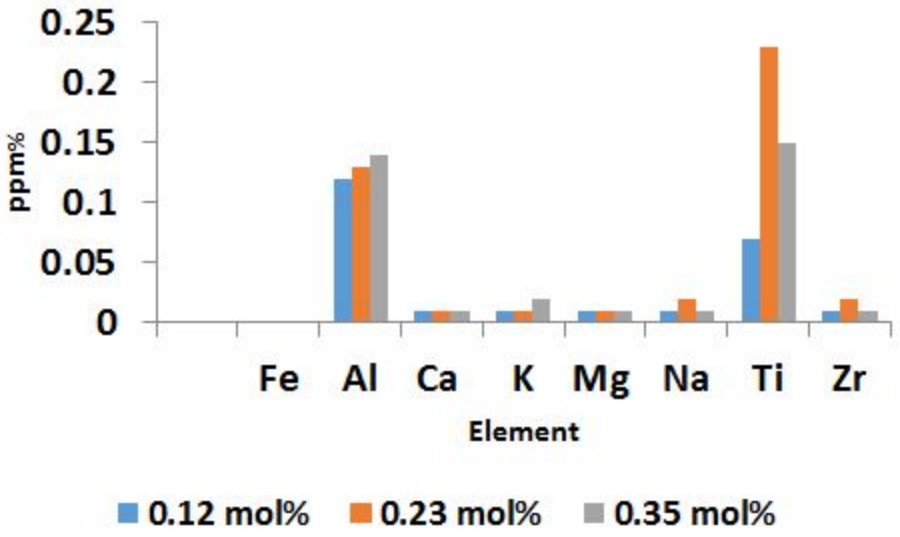

Figure 22 - *Results of ICPMS analysis on the titanium-doped samples prepared at Alcoa with larger amounts of aluminum and titanium present.*

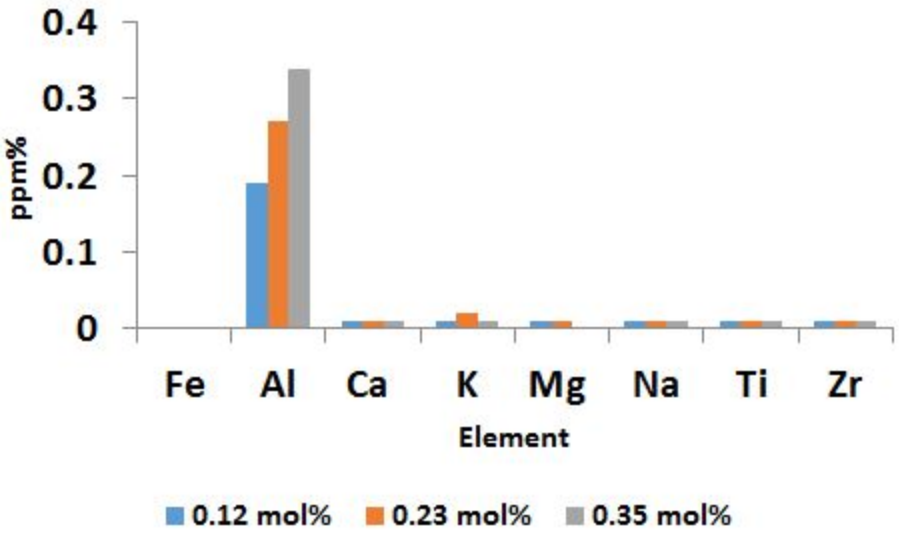

Figure 23 -*Results of ICPMS analysis on the alumina-doped samples prepared at Alcoa with double the amounts of aluminum present.*

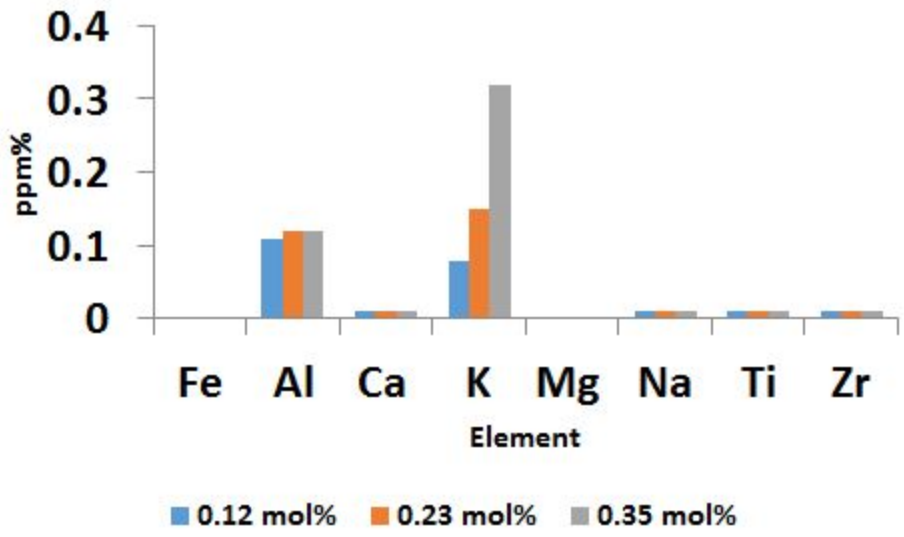

Figure 24 - *Results of ICPMS analysis on the potassia-doped samples prepared at Alcoa with amounts of aluminum and potassium present.*

6. Conclusion

This project analyzed the effects of trace amounts of titania, alumina and potassia as dopants in the cristobalite phase of SiO_2. Additionally, the effect of different processing techniques (ball milling and v-cone milling with alumina and silicon nitride milling media, respectively) on devitrification of fused silica into cristobalite were analyzed as well. HTXRD was used to analyze the phase transformations and intensity of amorphous silica versus cristobalite. ICPMS was used to give a precise elemental composition of the samples and to see if any contamination from the milling media was being added. Data analysis through two analytical programs showed that potassia has a significant effect on the cristobalite growth while alumina and titania did not. There was not any evidence to suggest that the media of the ball milling made any significant difference in devitrification. Finally, the experiment highlighted the need for an accurate method for determining of crystalline versus amorphous content for Aloca Howmet in the future.

7. Appendix

Table 3- *Samples with corresponding concentrations prepared for experimental analysis. Column two gives the atomic percentages of metal oxides found in the samples. The final three columns are the amounts of fused silica, cristobalite, and impurity used in a 200 g sample mixture, calculated using Eq. 1.*

Compound	Molar %	Fused Silica (g)	Cristobalite (g)	Impurity (g)
TiO_2	0.0012	170.290	29.402	0.307
TiO_2	0.0023	170.028	29.357	0.615
TiO_2	0.0035	169.766	29.312	0.922
Al_2O_3	0.0012	170.218	29.390	0.392
Al_2O_3	0.0023	169.884	29.332	0.784
Al_2O_3	0.0035	169.550	29.275	1.175
$KHCO_3$	0.0012	170.224	29.391	0.385
$KHCO_3$	0.0023	169.896	29.334	0.770
$KHCO_3$	0.0035	169.568	29.278	1.154

Data Analysis Code - *An R script that takes the HTXRD data as input, matches the background with a function of form 1/angle, subtracts the background from the profile, integrates the largest peak and the area around it, integrates just the peak, and outputs the ratio of the peak integration to the whole integration. This runs on every sample and every run for each sample. It also outputs the data at each stage, and a plot displaying its actions. Executed in R.*

```
setwd('/home/samuel/Documents/MSE/489')
smpl<-c('Ti-0.35-Alcoa','Al-0.35-Alcoa','K-0.12-Alcoa','K-0.23-Alcoa','K-0.35-Alcoa','K-0.35')
runs<-c('I4.xy','I6.xy','I8.xy','I10.xy','I12.xy','I14.xy','I16.xy','I18.xy','I20.xy') # Runs above alpha-beta transition temp
tmps<-c('1_440C','2_860C','3_1121C','4_1121C','5_1121C','6_1121C','7_1121C','8_1121C','9_701C')

peakIntensities <- NULL
peakRatios <- NULL
humpRatios <- NULL

for(s in 1:length(smpl)){
  intePeak <- NULL
  inteRatioPB <- NULL
  inteRatioHB <- NULL


  for(r in 1:length(runs)){

    # Load sample[s], run[r]
    data<-read.table(paste0(smpl[s],'/',runs[r]))
    colnames(data)<-c('ang','int')

    # Remove the area associated with the peak and the amophous hump that  to peak
    rmpeak<-(which.max(data$int)-350):(which.max(data$int)+350)


    # Regression on data without peak and hump
    ang=data$ang[-rmpeak]
    invang=1/ang
    int=data$int[-rmpeak]
    regr=lm(int ~ invang)

    # Find line that represents background
    bgr<-regr$coefficients[1] + regr$coefficients[2]/data$ang

    # Data with background removed
    mod1<-data.frame(data$ang,data$int-bgr) # Notation for Modified Data 1

    # Find the edges of the peak
    # Linear regression of each side of the peak
    peakPos <- which.max(data$int)

    peakLeftAng <- (peakPos-20):peakPos
    peakLeftInt <- mod1[peakLeftAng,2]
```

```
    peakLeftFit <- lm(peakLeftInt[14:21] ~ peakLeftAng[14:21])

    peakRightAng <- peakPos:(peakPos+20)
    peakRightInt <- mod1[peakRightAng,2]
    peakRightFit <- lm(peakRightInt[1:8] ~ peakRightAng[1:8])

    # Make regression line for each side of peak
    lineLeft <- data.frame(mod1[(peakPos-20):(peakPos+5),1],(peakLeftFit$coefficients[1] +
peakLeftFit$coefficients[2]*(peakPos-20):(peakPos+5)))
    lineRight <- data.frame(mod1[(peakPos-5):(peakPos+20),1],(peakRightFit$coefficients[1] +
peakRightFit$coefficients[2]*(peakPos-5):(peakPos+20)))

    # Determine edges by finding point of divergence from each line of fit
    leftEdge <- NA
    rightEdge <- NA
    stop <- 0
    for (i in 1:length(peakLeftAng)){
      if (abs(peakLeftInt[i]-lineLeft[(21-length(peakLeftAng)+i),2])<=300 & stop==0){
        leftEdge <- c((peakLeftAng[i]-3),mod1[(peakLeftAng[i]-8),2])
        stop <- 1
      }
    }

    stop <- 0
    for (i in 1:length(peakRightAng)){
      if (abs(peakRightInt[i]-lineRight[(5+i),2])>=300 & stop==0){
        rightEdge <- c((peakRightAng[i]+2),mod1[(peakRightAng[i]+7),2])
        stop <- 1
      }
      if (i==length(peakRightAng) & is.na(rightEdge)){ ## Special case for s=1 r=2
        rightEdge <- c((peakRightAng[12]+2),mod1[(peakRightAng[12]+7),2])
      }
    }
    cutLine <-
data.frame(data$ang[((leftEdge[1]-15):(rightEdge[1]+15))],rep(min(leftEdge[2],rightEdge[2]),length((leftEdge[1]-15):(rightEdge[1]
+15))))

    # Integrate peak and hump together and seperately
    inteBoth <- sum(mod1[(peakPos-450):(peakPos+450),2])
    mod2 <- data.frame(mod1[,1],(mod1[,2]-cutLine[1,2]))
    intePeak <- c(intePeak,sum(mod2[leftEdge[1]:rightEdge[1],2]))
    inteHump <- inteBoth-intePeak
    inteRatioPB = c(inteRatioPB,(100*intePeak[r]/inteBoth))


    # Plots
    plot(data,type='l')
    title(paste0('Data with Background Function -- ',smpl[s],'_',tmps[r]))
    lines(data$ang,bgr,col='red')
    dev.copy(jpeg,paste0('Results/',smpl[s],'/BkgrLine_',tmps[r],'.jpeg'))
```

```
    dev.off()

    plot(data[-rmpeak,],type='l')
    title(paste0('Data with Background Function, without Peak -- ',smpl[s],'_',tmps[r]))
    lines(data$ang,bgr,col='red')
    dev.copy(jpeg,paste0('Results/',smpl[s],'/BkgrLineNoPeak_',tmps[r],'.jpeg'))
    dev.off()
    plot(mod1,type='l')

    title(paste0('Data with Background Removed -- ',smpl[s],'_',tmps[r]))
    dev.copy(jpeg,paste0('Results/',smpl[s],'/BkgrRemoved_',tmps[r],'.jpeg'))
    dev.off()

    plot(mod1,type='l')
    title(paste0('Data with Background Removed, Peak Fit -- ',smpl[s],'_',tmps[r]))
    lines(lineLeft,col='blue')
    lines(lineRight,col='blue')
    lines(cutLine,col='red')
    dev.copy(jpeg,paste0('Results/',smpl[s],'/BkgrRemovedPeakFit_',tmps[r],'.jpeg'))
    dev.off()

    # Save profiles
    write.csv(data,file=paste0('Results/',smpl[s],'/raw_',tmps[r],'.csv')) # Raw
    write.csv(data[-rmpeak,],file=paste0('Results/',smpl[s],'/NoPeak_',tmps[r],'.csv')) # Without selected peak
    write.csv(data.frame(data$ang,bgr),file=paste0('Results/',smpl[s],'/BackgroundCurve_',tmps[r],'.csv')) # Background fit values
    write.csv(mod1,file=paste0('Results/',smpl[s],'/WithoutBackground_',tmps[r],'.csv')) # Profile with background removed
  }

  # Outputs
  if (s==1){
    peakIntensities <- intePeak
    peakRatios <- inteRatioPB
  }else{
    peakIntensities <- data.frame(peakIntensities,intePeak)
    peakRatios <- data.frame(peakRatios,inteRatioPB)
  }

}
colnames(peakIntensities) <- smpl
colnames(peakRatios) <- smpl

row.names(peakIntensities) <- tmps
row.names(peakRatios) <- tmps

write.csv(peakRatios,file=paste0('Results/peakRatios.csv'))
```

9. References

1. Kingery, W.D., *Introduction to Ceramics*. 2nd ed. 1976: Wiley.
2. Pradyumna, R.B., Baig M. A. H., *Ceramic Cores for Turbine Blades: A Tooling Perspective*; D.D. Group, Editor., Defence Metallurgical Research Laboratory (DMRL).
3. NIST, *Phase Equilibria Diagrams Database*. 2016: National Institute of Standards and Technology.
4. Sosman, R.B., *The Phases of Silica*. 1965, New Brunswick NJ: Rutgers University Press.
5. Cleynen, O. *Jet Turbine Wax Pattern*; Available from: https://www.sulzer.com/hu/-/media/Media/Images/Corporate/News_and_Media/STR/2014/issue_1/gas_turbine_parts.jpg?bc=ffffff&mw=690.
6. Wikipedia, *Cristobalite*; Available from https://en.wikipedia.org/wiki/Cristobalite.
7. Kirex Techno, *Lost Wax Casting*; Available from: http://casting.kirextechno.com/en/wp-content/uploads/2014/12/INVESTMENT-CASTING-PROVESS.jpg.
8. Sickafus, K. (2016). *Quick Introduction to the Structure of Glasses.* University of Tennessee-Knoxville.
9. Jagiellonian University (2016). *Innovative Laboratory of Functional Materials and Catalysis;* Available from:http://www.atomin.uj.edu.pl/aparatura/laboratorium-innowacyjnych-materialow-funkcjonalnych-i-katalitycznych.
10. San Roman, D., (2015). *Cristobalite Heating Pattern*.
11. Wyckoff, R. W. G. (1925). *The crystal structure of the high temperature form of cristobalite*; American Journal of Science **5**(1): 1921-1938.
12. Dollase, W.A., (1965). *Reinvestigation of the structure of low Cristobalite.* Zeitschrift fuer Kristallographie, Kristallgeometrie, Kristallphysik, Kristallchemie: p. 144.
13. Baur, W. H., Khan, A.A. (1971). *Rutile-type compounds. VI. Si O2, Ge O2 and a comparison with other rutile-type structures*. Acta Crystallographica 24: p. 2133-2139.
14. Ishizawa, N., Miyata, T.; Minato, I.; Marumo, F.; Iwai, S.I. (1980). *A structural investigation of alpha-Al2 O3 at 2170K*. Acta Crystallographica 36: p. 228-230.
15. Thomas, J. O.; Tellgren, R.; Olovsson, I. (1974). *Hydrogen-bond studies. LXXXIV. An X-ray diffraction study of the structures of K H C O3 and K D C O3 at 298, 219, 95 K*. Acta Crystallographica 30: p. 1155-1166.